Supporting Information

Srivastava *et al.* 10.1073/pnas.0805163105

SI Materials and Methods

MD Simulations. For CpHMD stimulations, the system first was energy-minimized by using six consecutive rounds of 800 steps of the steepest descent algorithm followed by 1,200 steps of the conjugate gradient algorithm giving a total of 12,000 steps. Harmonic restraints applied to the alpha carbons were slowly relaxed from 25 to 1 kcal/mol/A^2 by the end of the energy minimization step. To save computational time, a 15-Å cutoff for nonbonded interactions was used. The equilibration period in the molecular dynamics (MD) simulations consisted of three stages. In the first one, the system was gradually heated to 300 K for 30 ps at 100-K intervals followed by 70 ps at 300 K. The remaining restraints were gradually reduced to zero in this stage. The second stage consisted of 50 ps of unrestrained equilibration. Finally, in the third stage, the constant pH MD (CPHMD) approach was applied (1). The method implemented in AMBER addresses the dynamic dependence of pK_a through Monte Carlo sampling of the Boltzmann distribution of protonation states concurrent with the MD simulations. The nature of the distribution is affected by solvent pH, which is set as an external parameter. In the final equilibration stage, the pH variable was defined and the system was submitted to a MD run of 20 ps. The salt concentration was set at 0.1 M. The MD run was then continued for 10 ns at conditions of low pH (6.0) and high pH (8.0). Solute temperature was weakly coupled to a Berendsen temperature bath (2) at 300 K with a time constant of 2 ps. Bond lengths including hydrogen were constrained by using the SHAKE algorithm (3). The time step was 1 fs. The center-of-mass motion was removed at regular intervals of 1,000 fs. The trajectories were saved every 1 ps. In the MD simulations, the cutoff for nonbonded interactions was 12 Å.

Principal component analysis (PCA) was carried out to further analyze the molecular dynamics results for both wild-type and H2418F mutant trajectories. Cartesian coordinates of all backbone atoms or all heavy atoms in the actin binding site were used for the PCA analysis. The trajectories from all four simulations were concatenated for the PCA analysis, such that the principal components represent the major differences among the trajectories, in addition to the variation within each trajectory. The results (Fig. S1) highlight that (*i*) large conformational changes are observed in wild type between pH 6.0 and 8.0; (*ii*) the wild type and H2418F mutant are similar at pH 8.0; and (*iii*) the conformational changes observed in H2418F as a function of pH are different from those of the wild-type protein.

NMR. The mouse talin USH-I/LWEQ domain (2300–2501) was expressed as a translational fusion to the C terminus of GST, with an intervening PreScission protease recognition site. GST-talin was purified from the soluble cell fraction using glutathione affinity chromatography and cleaved on-column with PreScission protease (GE Healthcare Biosciences) in buffer (50 mM KH_2PO_4/1 mM DTT/1 mM EDTA) at 4°C overnight. Recombinant talin USH-I/LWEQ was eluted and concentrated to 1 mM. Expression of talin USH-I/LWEQ as a PreScission-cleavable GST fusion protein results in the purified protein having two nonnative residues, Gly-Pro, appended to the N terminus; the recombinant talin USH-I/LWEQ thus contains 203 residues.

Experiments were performed on Bruker DRX 500 and Avance 800-MHz spectrometers. Data were processed by using the Azara suite of programs, provided by Wayne Boucher and the Department of Biochemistry, University of Cambridge (Cambridge, UK) (http://www.bio.cam.ac.uk/azara). Spectra were analyzed by using ANSIG (4). Initial $^1H^N$, ^{15}N, $^{13}C\alpha$, $^{13}C\beta$, and $^{13}C'$ backbone resonance assignments of a shorter talin USH-I/LWEQ construct lacking the dimerization helix (2300–2482) were made at 318 K and pH 6.0 by using standard 3D triple-resonance experiments (5). Resonance assignments obtained at 318 K were transferred to spectra of a longer talin USH-I/LWEQ construct (2300–2501) at 305 K by using standard 3D triple-resonance experiments and 3D ^{15}N-edited NOESY spectra [HNCA, HN(CO)CA, HN(CO)CA, HNCACB, CBCA-(CO)NH, 15N-edited NOESY-HSQC, ^{15}N-, ^{15}N-edited HSQC-NOESY-HSQC (6)].

Video Microscopy. For fluorescence imaging, cells were plated on 15-mm glass coverslips for 24 h to achieve a monolayer, the monolayer was scored with a P20 pipette tip and washed with medium, and cells were used 6–8 h after wounding. To sustain activity of HCO_3^- transporters during imaging, cells were maintained in DMEM containing 25 mM $NaHCO_3$ within an environmentally controlled chamber at 37°C and 5% CO_2. Images were acquired at 30-s intervals for 60 min with a ×100/1.49 NA Apo objective lens on a microscope (model TE-2000 pfs; Nikon) equipped with a spinning disk confocal scan head (CSU10; Yokogawa) and a cooled charged-coupled device camera (cool-SNAP HQ2; Photometrics). Bright-field imaging was performed and recorded as described previously (7).

Extending lamellipodia in cells expressing fluorescent-tagged proteins were selected in the mid-stack of movies to capture their assembly and disassembly. Image J software was used to outline focal adhesions, and an equal area juxtaposed was selected for background fluorescence intensity. Focal adhesion lifetime was measured as the time from frame of background-subtracted adhesion (fluorescence signal) formation to the frame of its disappearance. For each movie measurements were obtained for 10–15 individual adhesions on four to six cells. The area outlining focal adhesions was recorded as the size. Statistical analysis was performed by using GraphPad software.

Immunoblotting. Cells were grown until a confluent monolayer and lysed in modified RIPA buffer. Normalized whole-cell lysates were resolved on 8% SDS/PAGE, and an anti-GFP antibody (Clontech) was used to detect GFP-talin and GFP-paxillin.

1. Mongan J, Case DA, McCammon JA (2004) Constant pH molecular dynamics in generalized Born implicit solvent. *J Comput Chem* 25:2038–2048.
2. Berendsen HJC, Postma JPM, van Gunsteren WF, DiNola A, Haak JR (1984) Molecular dynamics with coupling to an external bath. *J Chem Phys* 81:3684–3690.
3. Ryckaert J-P, Ciccotti G, Berendsen HJC (1977) Numerical integration of the Cartesian equations of motion of a system with constraints: Molecular dynamics of n-alkanes. *J Comput Phys* 23:327–341.
4. Kraulis PJ (1994) Solution structure and dynamics of ras p21.GDP determined by heteronuclear three- and four-dimensional NMR spectroscopy. *J Mol Biol* 243:696–718.
5. Gingras AR, *et al.* (2008) The structure of the C-terminal actin-binding domain of talin. *EMBO J* 27:458–469.
6. Sattler M, Schleucher J, Griesinger C (1999) Heteronuclear multidimensional NMR experiments for the structure determination of proteins in solution employing pulsed field gradients. *Prog NMR Spectrosc* 34:93–158.
7. Denker SP, Barber DL (2002) Cell migration requires both ion translocation and cytoskeletal anchoring by the Na-H exchanger NHE1. *J Cell Biol* 159:1087–1096.

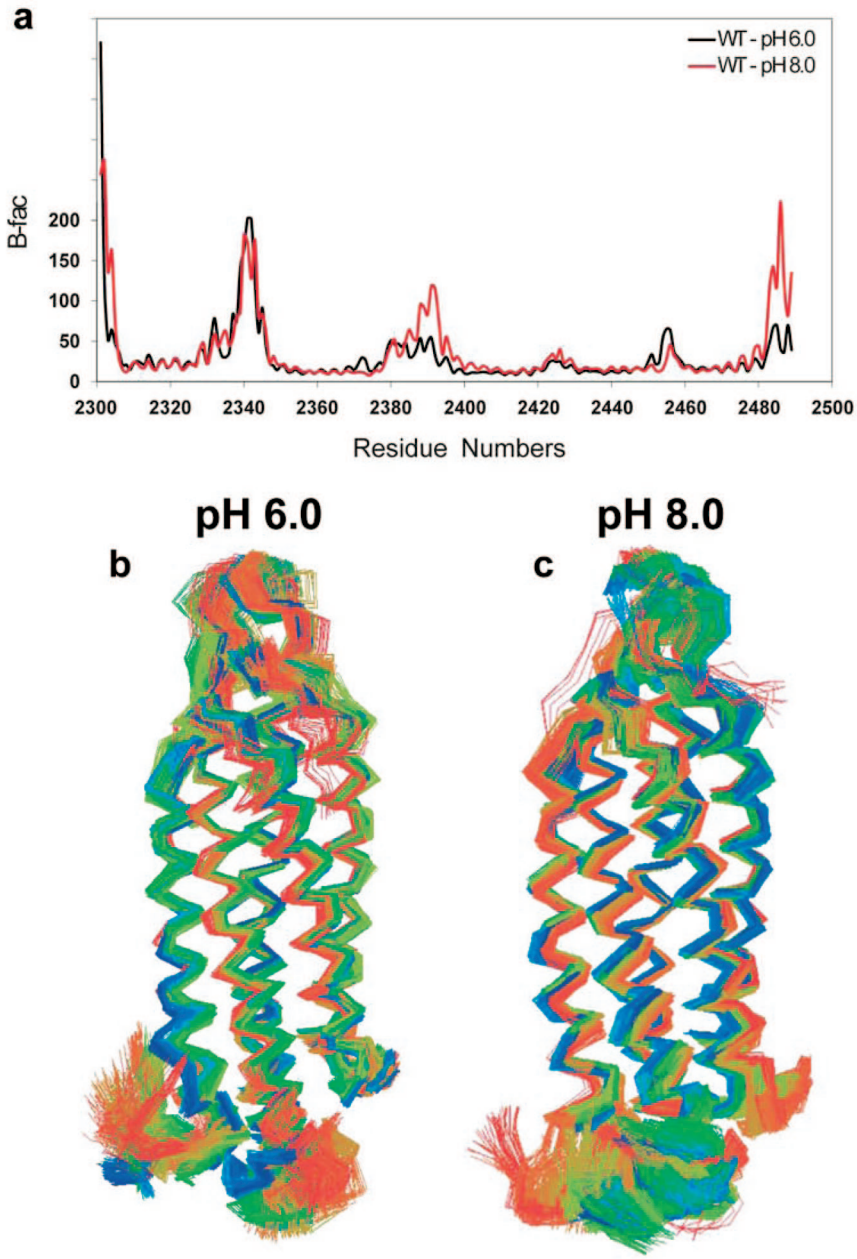

Fig. S1. Differences in structure and dynamics of talin USH-I/LEQ module between pH 6.0 and pH 8.0 mediated by changing protonation states. (*a*) Comparison of B factors on a per-residue basis from atom positional root mean square fluctuations on Cα atoms obtained from the final 500 ps of the MD simulations, wild-type talin at pH 6.0 (black) and pH 8.0 (red). The B factors are computed as $8\pi^2U^2$, where U is the mean-squared variation from the average structure, i.e., 1-Å rms fluctuation corresponds to a B factor of 79. (*b* and *c*) Configurations from the final 5 ns showing conformational changes over time (red corresponds to the beginning of the simulation, and blue corresponds to the end).

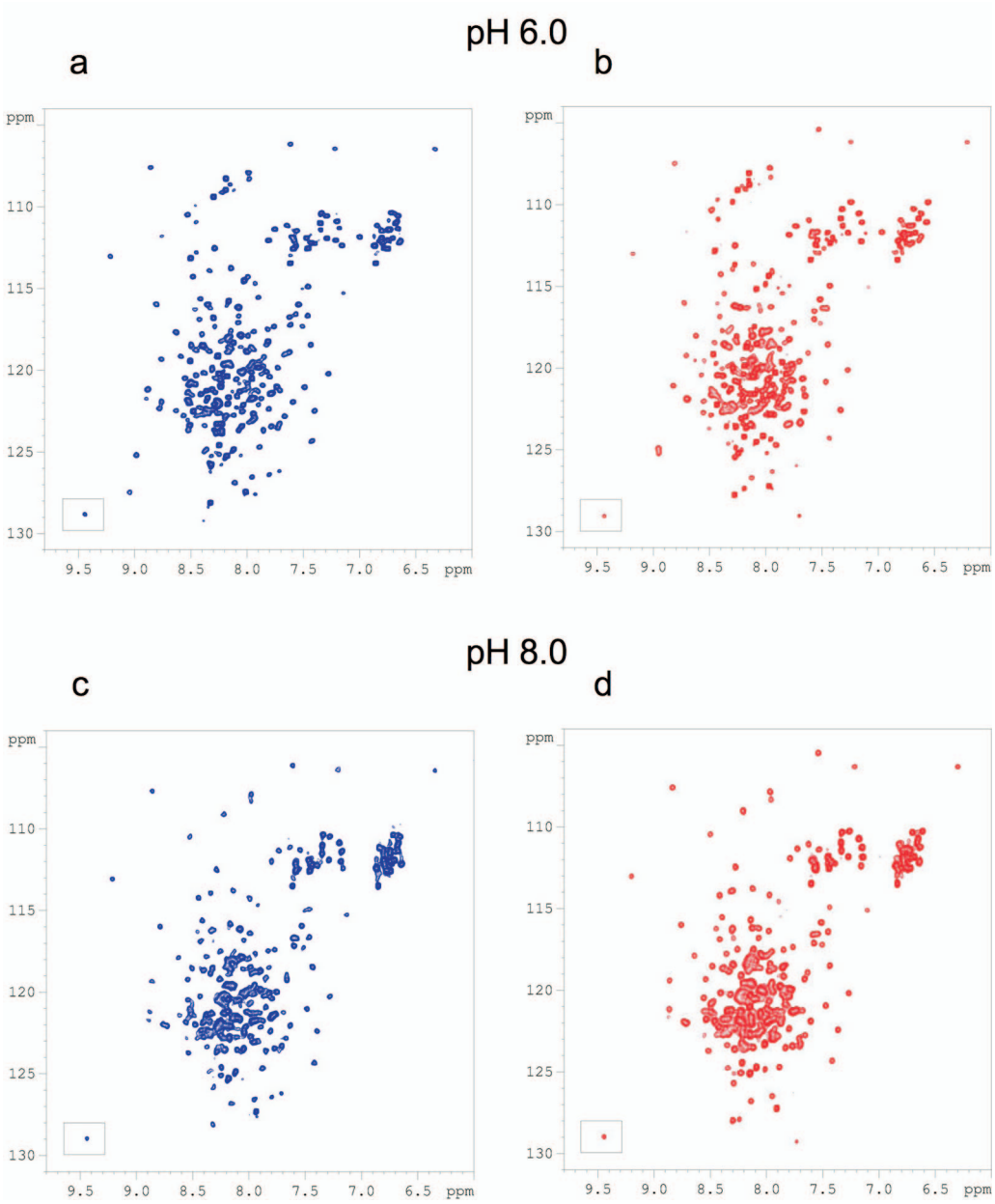

Fig. S2. 2D ^{15}N-HSQC spectra for wild-type talin (2300–2501) at pH 6.0 (*a*), H2418F mutant talin (2300–2501) at pH 6.0 (*b*), wild-type talin (2300–2501) at pH 8.0 (*c*), and H2418F mutant talin (2300–2501) at pH 8.0 (*d*). (*Inset*) The single tryptophan at 10.5 ppm (^{1}H).

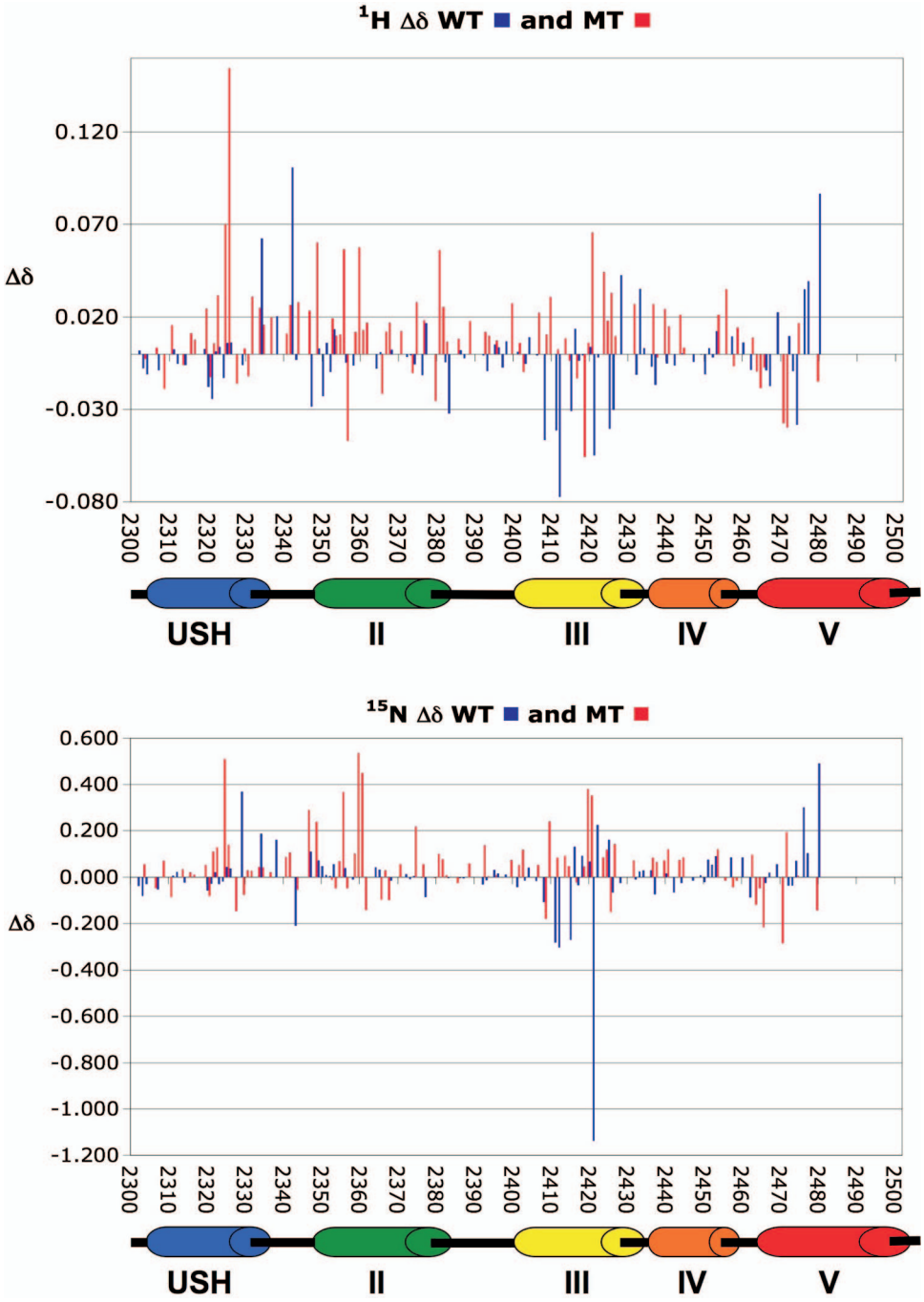

Fig. S3. Chemical shift changes at pH 6.0 versus pH 8.0 ($\Delta\delta_{TOT} = |\Delta^{1}H| + |\Delta^{15}N| \times 0.2$) along the linear sequence for wild-type dimeric talin USH-I/LWEQ (2300–2541) (*Upper*) and wild-type monomeric talin USH-I/LWEQ (2300–2501) (*Lower*). Secondary structure elements are indicated below.

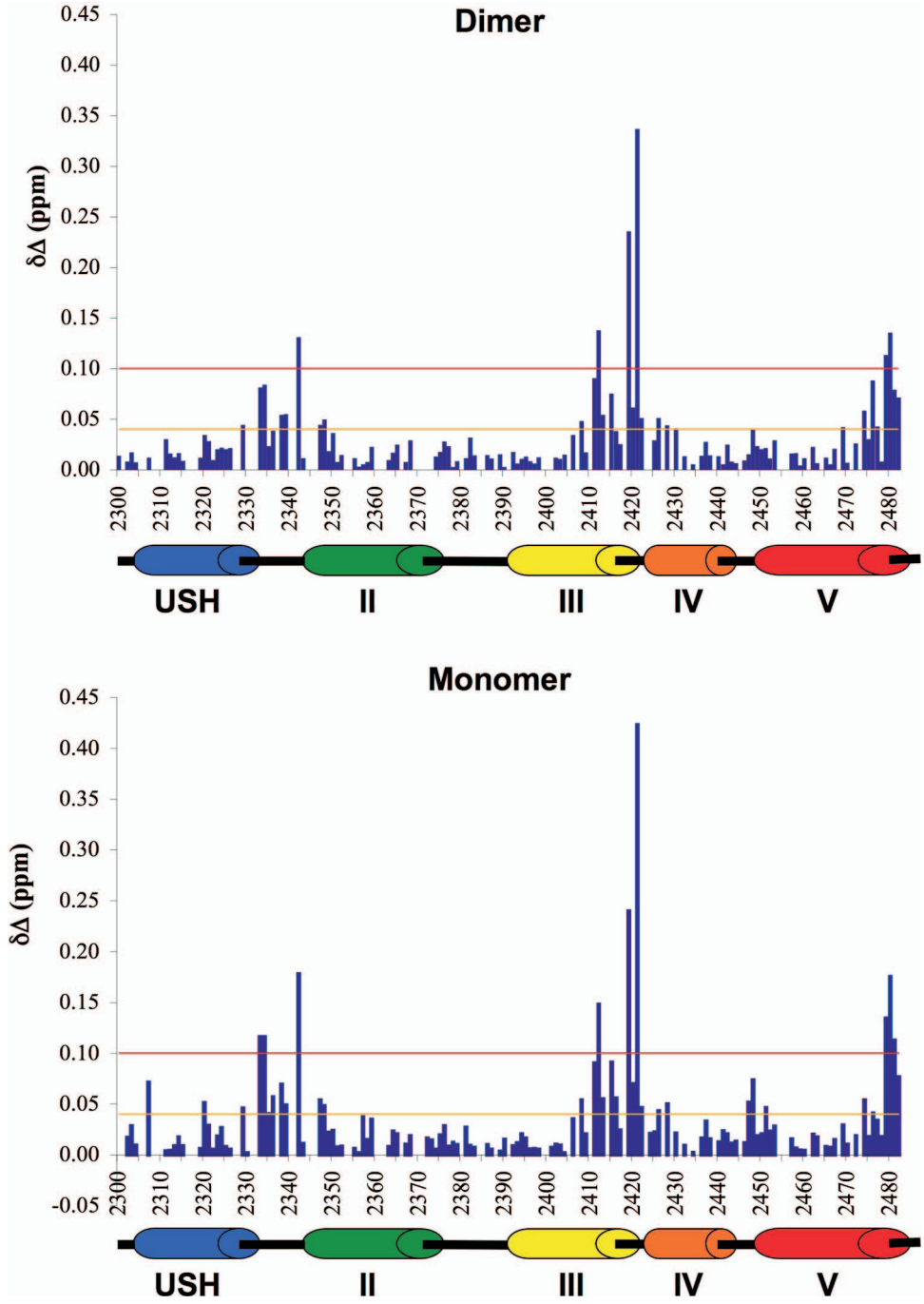

Fig. S4. Proton and ^{15}N chemical shift changes ($\Delta\delta$ pH 8.0 minus pH 6.0) along the linear sequence for wild-type (blue) and H2418F mutant (red) talin USH-I/LWEQ. Chemical shift changes for ^{1}HN (*Upper*) and ^{15}N (*Lower*) are shown separately. Secondary structure elements are indicated below.

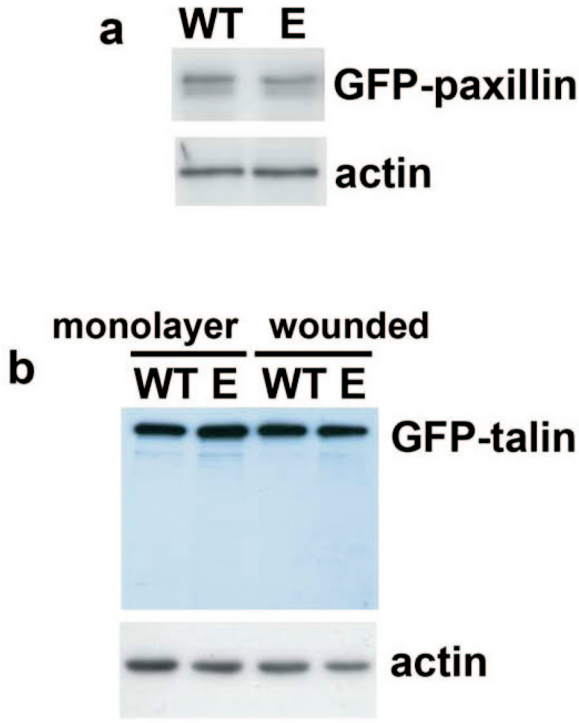

Fig. S5. Backbone (*a*) and actin binding site (*b*, heavy atoms) PCA plots.

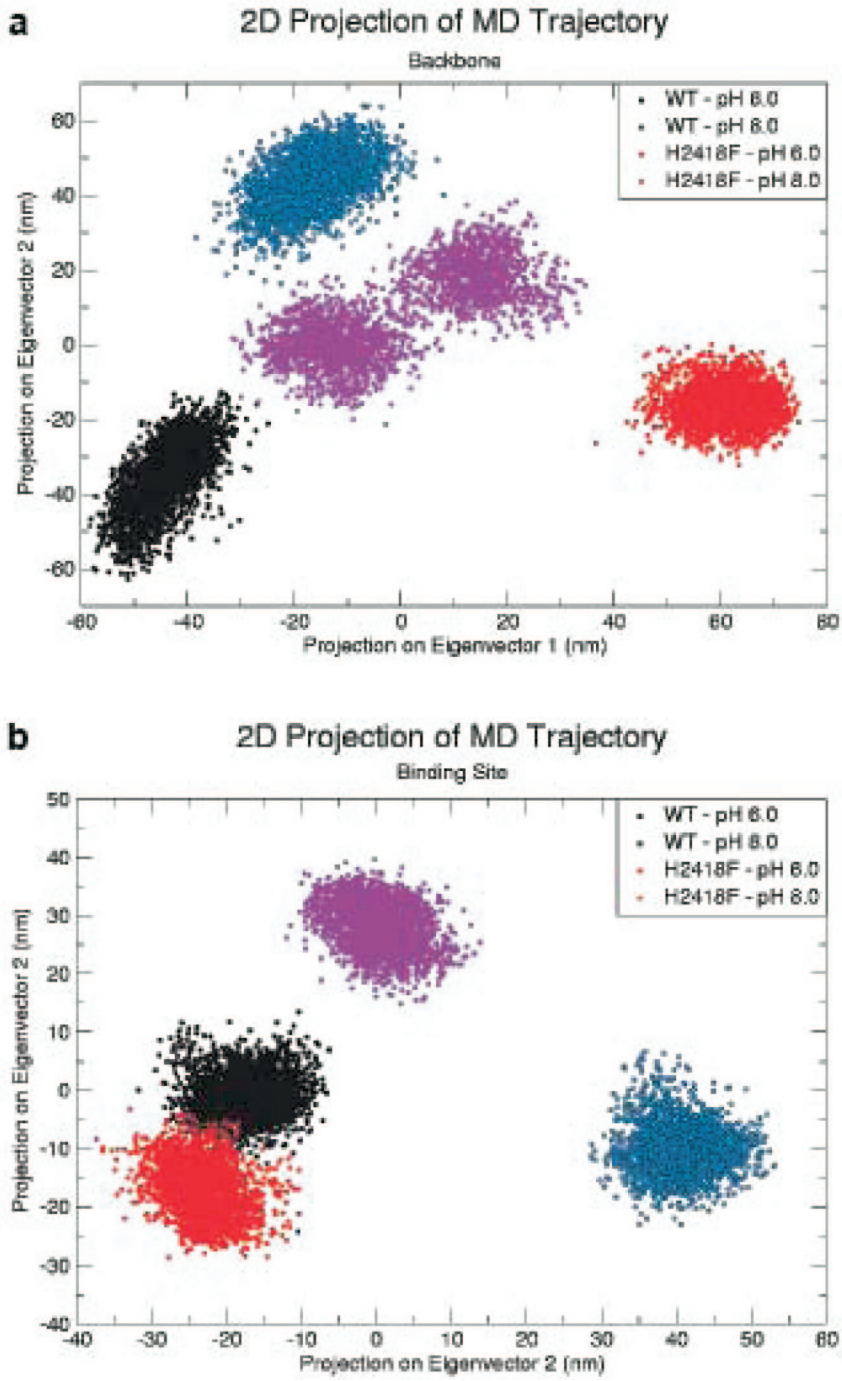

Fig. S6. (*a*) GFP-paxillin expression in WT and E266I cells. (*b*) GFP-talin expression in WT cells and E266I cells before and after 4-h wounding of a monolayer.

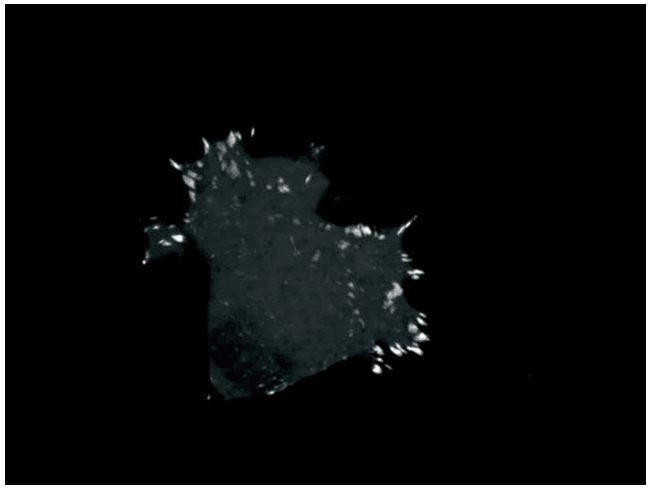

Movie S1. Time-lapse video microscopy of WT cells expressing GFP-paxillin at the wound edge 6 h after wounding. Images were captured at 30-s intervals for 60 min. Captured images were compiled into a QuickTime movie using Sorenson Video Compressor software.

Movie S1 (MOV)

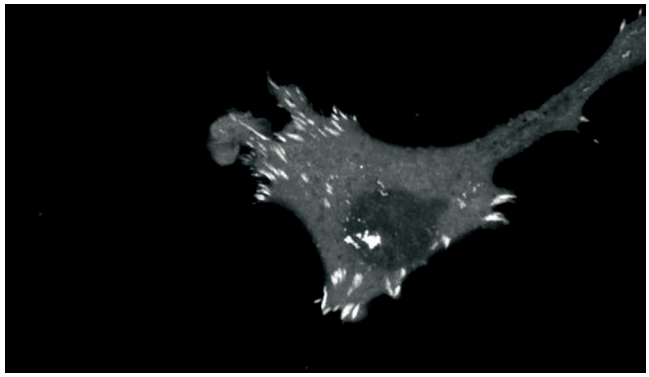

Movie S2. Time-lapse video microscopy of E266I cells expressing GFP-paxillin at the wound edge 6 h after wounding. Images were captured at 30-s intervals for 60 min. Captured images were compiled into a QuickTime movie using Sorenson Video Compressor software.

Movie S2 (MOV)

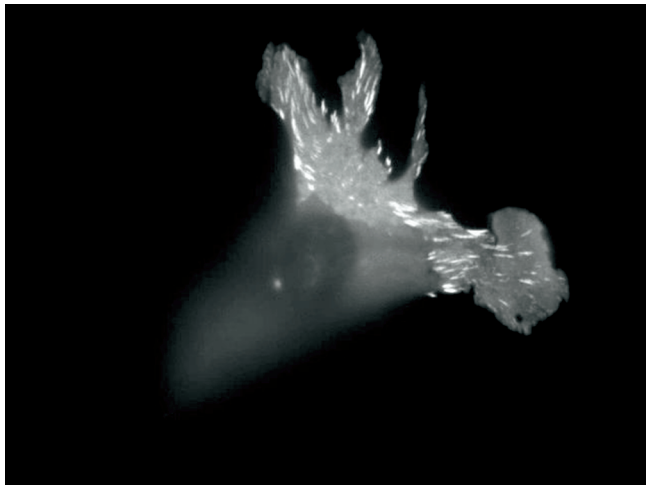

Movie S3. Time-lapse video microscopy of cherry-paxillin in WT cells expressing GFP-wild-type talin at the wound edge 6 h after wounding. Images were captured at 30-s intervals for 60 min. Captured images were compiled into a QuickTime movie using Sorenson Video Compressor software.

Movie S3 (MOV)

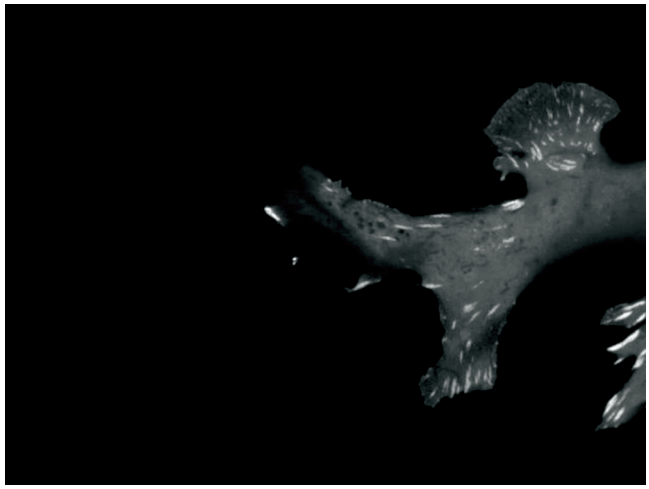

Movie S4. Time-lapse video microscopy of cherry-paxillin in WT cells expressing GFP-talin-H2418F at the wound edge 6 h after wounding. Images were captured at 30-s intervals for 60 min. Captured images were compiled into a QuickTime movie using Sorenson Video Compressor software.

Movie S4 (MOV)

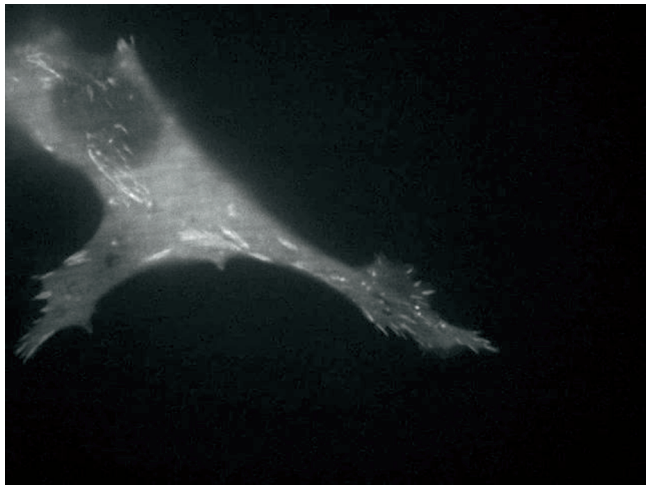

Movie S5. Time-lapse video microscopy of cherry-paxillin in E266I cells expressing GFP-wild-type talin at the wound edge 6 h after wounding. Images were captured at 30-s intervals for 60 min. Fluorescence visible in small motile vesicles is an artifact of cherry-red and was not seen in cells expressing GFP-paxillin. Captured images were compiled into a QuickTime movie using Sorenson Video Compressor software.

Movie S5 (MOV)

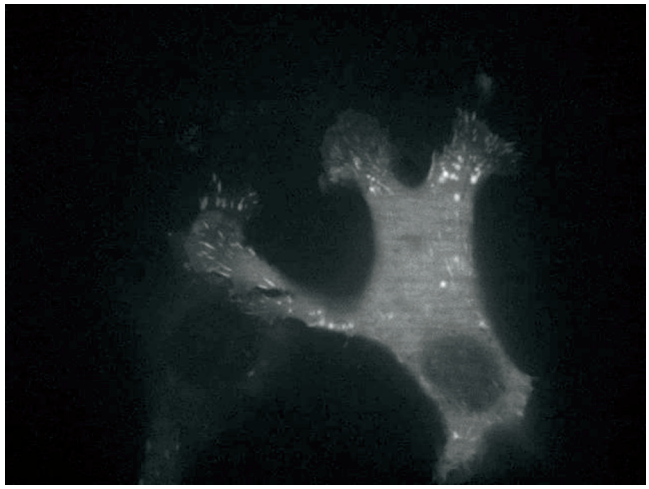

Movie S6. Time-lapse video microscopy of cherry-paxillin in E266I cells expressing GFP-talin-H2418F at the wound edge 6 h after wounding. Images were captured at 30-s intervals for 60 min. Fluorescence visible in small motile vesicles is an artifact of cherry-red and was not seen in cells expressing GFP-paxillin. Captured images were compiled into a QuickTime movie using Sorenson Video Compressor software.

Movie S6 (MOV)